

Amplitude determination for $MM \rightarrow MM$, $M = \pi, K$ and cross-sections for $\gamma\gamma \rightarrow \pi^+\pi^-, \pi^0\pi^0$ in a chiral model

S. P. Klevansky^{1*} and R. H. Lemmer^{2†}

¹*Institut für Theoretische Physik,
Universität Heidelberg, Philosophenweg 12,
69120 Heidelberg, Germany,
and*

²*School of Physics,
University of the Witwatersrand,
Johannesburg, Private Bag 3,
WITS 2050, South Africa.*

(Dated: July 29, 2016)

Recently Dai and Pennington have performed a comprehensive analysis of essentially all pion and kaon pair production data from two-photon collisions below 1.5 GeV, including all high statistics results from Belle, as well as the older data from Mark II at SLAC, CELLO at DESY, and Crystal Ball at SLAC. Imposing the basic constraints required by analyticity, unitarity, and crossing symmetry and making use of Low's low energy theorem for QED, they are able to extract the final-state strong-interaction scattering *amplitudes* for the intermediate $\pi\pi \rightarrow \pi\pi$ and $\pi\pi \rightarrow K\bar{K}$ reactions in a model-independent fashion. In addition, they provide good fits to the respective $\gamma\gamma \rightarrow \pi\pi$ cross-sections that are known in the low-energy sector in the restricted angular range, $|\cos\theta| < 0.6 - 0.8$. Using the parameters obtained in this fashion, these authors construct the $\gamma\gamma \rightarrow \pi\pi$ cross-sections integrated over the full angular range. In this work, we use a version of chiral perturbation theory developed by Oller and Oset to evaluate the final-state strong-interaction amplitudes directly theoretically and we compare our thus obtained low-energy QCD-based results directly with the amplitudes extracted by Dai and Pennington. We also calculate the $\gamma\gamma \rightarrow \pi\pi$ cross-sections (integrated over the full angular range) and compare these with those obtained by Dai and Pennington. This calculation thus gives a more detailed insight into the fit of chiral perturbation theory, not just to the measured $\gamma\gamma \rightarrow \pi\pi$ cross-sections, as is usually presented, but rather to a higher level of detail through the available analysis of the experimental data for the underlying final-state strong-interaction meson-meson scattering amplitudes $\pi\pi \rightarrow \pi\pi$ and $\pi\pi \rightarrow K\bar{K}$ themselves. The fits appear to be reasonable over the energy range considered.

PACS numbers: 11.10.St, 11.30.Rd, 13.75.Lb

[†] deceased

*Electronic address: spk@physik.uni-heidelberg.de

I. INTRODUCTION

Photon-photon to meson-meson cross-sections have been measured by several experimental groups over the last decades [1–11]. The high statistics experimental data obtained by the Belle Collaboration at KeKB for $\gamma\gamma \rightarrow \pi^+\pi^-$ [1], $\gamma\gamma \rightarrow \pi^0\pi^0$ [2] and $\gamma\gamma \rightarrow \pi^0\eta$ [3] cross-sections, plus the similar high quality data for $\gamma\gamma \rightarrow K^+K^-$ and $\gamma\gamma \rightarrow K^0\bar{K}^0$ for $\gamma\gamma$ center-of-mass collision energies up to ~ 1 GeV [8–10] have given new impetus to the field and can provide important new information with which to probe the possible quark structure of the light isoscalar $f_0(500)$, $f_0(980)$ and isovector $a_0(980)$ scalar mesons [12, 13]. Recently, Dai and Pennington have performed a comprehensive amplitude analysis of the processes $\gamma\gamma \rightarrow \pi^+\pi^-$, $\pi^0\pi^0$ and $K\bar{K}$ below 1.5 GeV [14]. Using all available experimental data, they have extracted the associated final-state strong-interaction transition matrices, $\pi\pi \rightarrow \pi^+\pi^-$, $\pi^0\pi^0$, $K\bar{K}$ in a model-independent fashion, using only properties of analyticity, unitarity and crossing symmetry, and Low’s low energy theorem for QED. Their fits pertain to the experimental data that are measured over a restricted angular range, $|\cos\theta| < 0.6 - 0.8$. Having determined all parameters, they are able to construct the cross-sections for $\gamma\gamma \rightarrow \pi^+\pi^-$, $\pi^0\pi^0$ that would be expected after integrating over the full angular range.

Such developments open up several intriguing possibilities from a theoretical point of view. (a) First, the precise knowledge of the final-state strong-interaction transition matrices can be used to test the predictions of low-energy QCD, or at least differentiate between various models thereof. (b) In the energy range studied, it opens up the possibility of examining the viability of detailed combined structures that potentially can form. Various strong-interaction models with different structural properties have already been explored in some detail for the light isoscalar and isovector mesons. These include, for example, descriptions with simple $q\bar{q}$ pairs [15–19], more complex $q^2\bar{q}^2$ states [20] or a $K\bar{K}$ molecular structure [21–27] for the $f_0(980)$ and $a_0(980)$ in particular. Now, in addition to the strong interaction, which is known through the analysis of [14], electromagnetic effects can be incorporated, and, for example, the resonance formed in the production and subsequent decay of the K^+K^- hadronic atom kaonium [28–31] can be studied theoretically. This, in turn, may become accessible experimentally.

The aim of the present paper is to examine (a) above, and to determine how well chiral perturbation theory (CHPT) [32, 33], taken together with QED to calculate the final-state strong-interaction and electromagnetic transition matrices serves to give a good description of the final-state strong-interaction transition matrices as compared with the model-independent curves extracted by Dai and Pennington from experiment [14]. Our calculated final-state strong-interaction transition matrices turn out both qualitatively and quantitatively to be in reasonable agreement for both the individual real and imaginary parts. We also calculate the full cross-sections for the $\gamma\gamma \rightarrow \pi^+\pi^-$ and $\pi^0\pi^0$ reactions, incorporating the electromagnetic contributions, and again find a reasonable, but not perfect, agreement with the extracted curves of Dai and Pennington. We leave the question of new structures such as the presence of kaonic atoms appearing in the cross-section, which requires a solid knowledge of the strong-interaction transition matrices, as presented here, to a forthcoming article.

For our aims, both for evaluating the full transition matrices, and for calculating the light-light to meson pair cross-sections we require a detailed analysis of the underlying electromagnetic interaction as well as the strong interaction component through meson–meson scattering processes. Such studies are not new. In particular, Oller and Oset [34] extract meson–meson interactions within the pseudoscalar meson $SU(3)$ flavor octet from the Lagrangian given by leading order CHPT [32, 33] as the appropriate theoretical realization of low energy QCD. They then use these interactions as input for the Lippmann–Schwinger equation to provide a non-perturbative calculation of the pseudoscalar meson–meson scattering and reaction amplitudes. We will follow this approach here.

It is, however, important to bear in mind that the validity of the leading order CHPT results are restricted to center-of-mass collision energies up to $\sim \mathcal{O}(1 \text{ GeV})$. A glance at the two-photon collision data [1–3] shows that, while the $f_0(500)$, $f_0(980)$ and $a_0(980)$ again appear quite naturally in the CHPT calculations as dynamically generated resonances [35] below 1 GeV center-of-mass total energy, with energies and widths compatible with experiment in the total cross-section of the relevant reaction channels, the dominance of the wide $f_2(1270)$ and $a_2(1302)$ resonances eventually overshadow the CHPT contribution at higher energies. Whilst not important for studying the $\gamma\gamma \rightarrow$ kaonium production process, we remark that when the CHPT transition amplitudes are supplemented by contributions from the above two resonances in parametrized form [36], both being interpreted as d -wave, helicity $\lambda = 2$ states, plus the exchange of vector and axial vector octet resonances in the u and t channels [37], there is good agreement with the available photon-photon collision data over the entire energy range from the two-meson threshold to $\sim 1.4 \text{ MeV}$ in the center-of-mass system.

This article is arranged as follows: Section II addresses the calculation of the T -matrices for the photon-photon interactions. In Subsections IIA, IIB and II C, we build up the Born contributions, the contributions containing meson-meson scattering through CHPT and the resonant and axial contributions that cannot be described by CHPT, respectively. These are collated in Subsection IID. In Section III, we compare our calculated amplitudes and cross-sections with the extracted fits of [14] and experimental results. We summarize and conclude in Section IV.

II. PRODUCTION AMPLITUDES FOR THE PROCESSES $\gamma\gamma \rightarrow \pi^+\pi^-$, $\pi^0\pi^0$ AND K^+K^-

The theoretical basis for evaluating the $\gamma\gamma \rightarrow m_1m_2$ processes has been studied in different contexts or models before, see for example [14, 35] and references cited therein, and involves both the electromagnetic coupling of the photons to (charged) mesons that is determined through QED, as well as quantum chromodynamics (QCD) for the final-state strong interactions between the mesons themselves. As the latter cannot be extracted directly from QCD itself, we use CHPT as an appropriate realisation of the strong interactions in the low-energy sector. These processes are represented graphically in Fig. 1 by the Feynman diagrams for the $\gamma\gamma \rightarrow m_1m_2$ transition amplitude for incoming photon four-momenta and helicities (q_1, λ_1) and (q_2, λ_2) leading to outgoing mesons with four-momenta (p_1, p_2) . The filled circle diagram in Fig. 1 a) denotes the full transition amplitude tensor $iT_{\gamma\gamma \rightarrow m_1m_2}^{\mu\nu}$. This itself is resolved into two parts: a direct coupling of the electromagnetic interaction to the mesons plus a term in which both the electromagnetic and strong interactions play a role. The first is the Born term $iT_{B;\gamma\gamma \rightarrow m_1m_2}^{\mu\nu}$, denoted in the figure as an open circle, and is only present when photons couple to charged meson pairs m_+m_- in the final state. The second diagram, denoted as $iT_{S;\gamma\gamma \rightarrow m_1m_2}^{\mu\nu}$, includes the contribution from the strong meson-meson interactions in the final state. The direct coupling of the electromagnetic interaction to the mesons via the Born term is again broken down into three individual terms, also shown in this figure, see b), and which contain one-meson exchange.

As it stands, low-energy CHPT does not account sufficiently for the $f_2(1270)$ and $a_2(1302)$ resonances, which have large widths that extend well into the region below 1.0 GeV. These are accommodated in our formalism via parametrization. We thus proceed as follows: in subsection A, we start with the Born term, in order to set our notation. We then evaluate contributions from the final-state strong interaction using CHPT in subsection B. In subsection C, we give the parametrization for resonant or axial, non-CHPT terms. Then, in subsection D, we build up the full T -matrix, that consists of the amplitudes

$$T_{\gamma\gamma \rightarrow m_1m_2}^{\mu\nu} = T_{B;\gamma\gamma \rightarrow m_1m_2}^{\mu\nu} + T_{S;\gamma\gamma \rightarrow m_1m_2}^{\mu\nu} + T_{R(A);\gamma\gamma \rightarrow m_1m_2}^{\mu\nu} \quad (1)$$

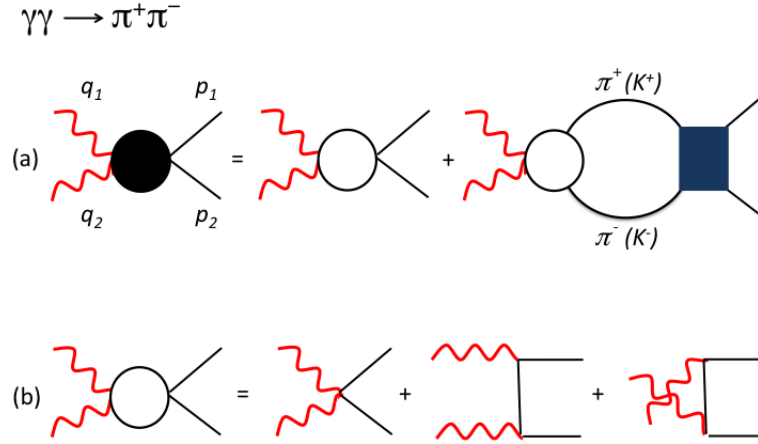


FIG. 1: [Color online] Scattering amplitudes for $\gamma(q_1) + \gamma(q_2) \rightarrow m_1(p_1) + m_2(p_2)$ collisions producing meson pairs of masses (m_1, m_2) with incoming and outgoing momenta (q_1, q_2) and (p_1, p_2) respectively. (a) The full amplitude (filled circle). This amplitude includes strong interactions in the final state as given by the 4-point meson-meson scattering T -matrix (filled box diagram). (b) The Born term (open circle) only involves the electromagnetic coupling vertices of photons to charged mesons and is only present for $\pi^+\pi^-$ or K^+K^- in the final state.

with $\mu, \nu = 0..3$, and specify the cross-sections. Throughout this work, we use natural units, where $\hbar = c = 1$ and the charge $e^2/4\pi = \alpha$.

A. Electromagnetic contributions to $\gamma\gamma \rightarrow m^+m^-$ in the helicity basis

As the process $\gamma\gamma \rightarrow \pi^+\pi^-$ due to electromagnetic interactions (Born approximation) has been well-studied in the literature, see for example [37], we provide only a concise summary of important results here. These are directly applicable to the process $\gamma\gamma \rightarrow K^+K^-$. In general, the transition amplitude in the Born approximation corresponding to the first diagram of Fig. 1a), or all diagrams in Fig. 1b) leads to the expression

$$T_{B;\gamma\gamma \rightarrow m^+m^-}^{\mu\nu} = e^2 \left\{ 2g^{\mu\nu} + \left[\frac{(2p_1 - q_1)^\mu (2p_2 - q_2)^\nu}{(p_1 - q_1)^2 - m_\pm^2} + (q_1 \rightarrow q_2, \mu \rightarrow \nu) \right] \right\}, \quad (2)$$

where m_\pm are the (common) masses of the final state mesons. This expression has to be contracted with polarization vectors ϵ_μ and ϵ_ν . For an explicit evaluation, (without loss of generality) we use a standard choice [38] $\epsilon_0 = 0$ and the 3-vectors of helicity λ_1, λ_2 , $\mathbf{e}_{\lambda_1}(1), \mathbf{e}_{\lambda_2}(2)$, both oriented along right-handed orthogonal axes xy perpendicular to the photon momentum vector in the z direction, $\mathbf{e}_{\lambda_1}(1) = \mathbf{i}, \mathbf{e}_{\lambda_2}(2) = \mathbf{j}$ and $\mathbf{e}_{\lambda_1}(1) \cdot \mathbf{e}_{\lambda_2}(2) = \delta_{\lambda_1, \lambda_2}$ to fulfil the Lorentz condition. This leads to the expression

$$(e_{\lambda_1}(1))_i T_{B;\gamma\gamma \rightarrow m^+m^-}^{ij} (e_{\lambda_2}(2))_j = -2e^2 \left\{ (\mathbf{e}_{\lambda_1}(1) \cdot \mathbf{e}_{\lambda_2}(2)) + \left[\frac{(\mathbf{p}_1 \cdot \mathbf{e}_{\lambda_1}(1))(\mathbf{p}_2 \cdot \mathbf{e}_{\lambda_2}(2))}{(p_1 \cdot q_1)} + \frac{(\mathbf{p}_2 \cdot \mathbf{e}_{\lambda_1}(1))(\mathbf{p}_1 \cdot \mathbf{e}_{\lambda_2}(2))}{(p_1 \cdot q_2)} \right] \right\}, \quad (3)$$

where the indices i, j can take on the values 1, 2, 3.

In the center-of-mass system, the incoming photon and outgoing meson lines in Fig. 1b) have four momenta $(q_1, q_2) = [\frac{1}{2}P_0, \pm \mathbf{q}]$ and $(p_1, p_2) = [\frac{1}{2}P_0, \pm \mathbf{p}]$ where $\sqrt{s} = P_0$ is the total collision energy. Using this, the contracted Born amplitude becomes

$$\begin{aligned} (T_{B;\gamma\gamma\rightarrow m^+m^-})_{\lambda_2\lambda_1} &= (e_{\lambda_2}^*(2))_i T_{B;\gamma\gamma\rightarrow m^+m^-}^{ij} (e_{\lambda_1}(1))_j \\ &= -2e^2 \left\{ (\mathbf{e}_{\lambda_2}^*(2) \cdot \mathbf{e}_{\lambda_1}(1)) - 2 \frac{(\mathbf{v} \cdot \mathbf{e}_{\lambda_2}^*(2))(\mathbf{v} \cdot \mathbf{e}_{\lambda_1}(1))}{1 - v^2 \cos^2 \theta} \right\}, \end{aligned} \quad (4)$$

where $\mathbf{e}_{\lambda_1}(1)$ is associated with particle 1 with incoming momentum \mathbf{q} and $\mathbf{e}_{\lambda_2}(2)$, with particle 2 with incoming momentum $-\mathbf{q}$. Also, the center-of-mass velocity is $v = 2p/P_0$, and $\cos \theta = \mathbf{p} \cdot \mathbf{q}/pq$ gives the polar angle of the scattering direction of the outgoing meson \mathbf{p} relative to the incoming photon \mathbf{q} . We choose to evaluate (4) for the Born amplitudes in the chiral helicity basis that is defined by $\mathbf{e}_{R,L}(i) = \mp \frac{1}{\sqrt{2}}(\mathbf{e}_1(i) \pm \mathbf{e}_2(i))$, $i = 1, 2$. Now one notes that in the center-of-mass system, the total helicity of the colliding photon pair can only take on the values $\lambda = 0$ or 2 , and this label is sufficient to characterize the contracted T -matrices, which we denote as $T^{(\lambda)}$. Then the individual (contracted) amplitudes are easily found [35] to be:

$$(T_{B;\gamma\gamma\rightarrow m^+m^-}^{(\lambda=0)})_{R(2)R(1)} = -(T_{B;\gamma\gamma\rightarrow m^+m^-}^{(\lambda=0)})_{L(2)L(1)} = -i \frac{2e^2(1-v^2)}{1-v^2 \cos^2 \theta}, \quad (5)$$

$$(T_{B;\gamma\gamma\rightarrow m^+m^-}^{(\lambda=2)})_{L(2)R(1)} = -(T_{B;\gamma\gamma\rightarrow m^+m^-}^{(\lambda=-2)})_{R(2)L(1)} = i \frac{2e^2 v^2 \sin^2 \theta e^{2i\phi}}{1-v^2 \cos^2 \theta}, \quad (6)$$

An expansion of the $T_{B;\gamma\gamma\rightarrow m^+m^-}^{(\lambda)}$ in spherical harmonics $Y_{J,\lambda}(\theta, \phi)$ for each total helicity λ yields the partial contracted amplitudes $T_{B;\gamma\gamma\rightarrow m^+m^-}^{(J,\lambda)}$, which can be used to identify the leading s - and d -wave contributions to (5) and (6). One finds

$$\begin{aligned} T_{B;\gamma\gamma\rightarrow m^+m^-}^{(0,0)} &= -2ie^2 \left[\frac{1-v^2}{2v} \ln \frac{1+v}{1-v} \right] \sqrt{4\pi} Y_{0,0} \\ T_{B;\gamma\gamma\rightarrow m^+m^-}^{(2,2)} &= 2ie^2 \left[-\frac{1}{v^2} + \frac{5}{3} + \frac{(1-v^2)^2}{2v^3} \ln \frac{1+v}{1-v} \right] \sqrt{\frac{15\pi}{2}} Y_{2,2}(\theta, \phi) \\ v &= p/q = \sqrt{1 - \frac{4m_{\pm}^2}{s}} \quad m_{\pm} = m_{\pi}, m_K \end{aligned} \quad (7)$$

Here we have dropped the chiral indices, which are no longer necessary. General expressions for $T_{B;\gamma\gamma\rightarrow m^+m^-}^{(J,0)}$ and $T_{B;\gamma\gamma\rightarrow m^+m^-}^{(J,2)}$ for all allowed $J \geq \Lambda$ are available in the Appendix, see (A.1) to (A.5). However, the leading-order partial-wave amplitudes given above together account [35] for $\sim 90\%$ of the calculated Born cross-section for $s \lesssim 1 \text{ GeV}^2$ and thus build a convenient working assumption.

While the T -matrices will be of direct interest to us, for completeness we note that the individual helicity cross-sections can be evaluated. For example, for the process $\gamma\gamma \rightarrow \pi^+\pi^-$, for helicity 0, the differential cross-section is

$$\begin{aligned} \frac{d\sigma_B^{(0)}(\gamma\gamma \rightarrow \pi^+\pi^-)}{d\Omega} &= \left(\frac{1}{2}\right) \frac{v}{64\pi^2 s} |(T_{B;\gamma\gamma\rightarrow\pi\pi}^{(\lambda=0)})_{R(1)R(2)}|^2 \\ &= \frac{\alpha^2 v}{2s} \frac{(1-v^2)^2}{(1-v^2 \cos^2 \theta)^2}, \end{aligned} \quad (8)$$

so that

$$\sigma_B^{(0)}(\gamma\gamma \rightarrow \pi^+\pi^-) = \frac{\alpha^2 v}{2s} \int_{4\pi} d\Omega \frac{(1-v^2)^2}{(1-v^2 \cos^2 \theta)^2} = 2\pi \frac{\alpha^2 v}{s} \left[\frac{(1-v^2)}{2} + \frac{(1-v^2)^2}{4v} \ln \frac{1+v}{1-v} \right]. \quad (9)$$

Likewise for helicity 2, one has

$$\sigma_B^{(2)}(\gamma\gamma \rightarrow \pi^+\pi^-) = \frac{\alpha^2 v}{2s} \int_{4\pi} d\Omega \frac{(v^2 \sin^2 \theta)^2}{(1 - v^2 \cos^2 \theta)^2} = 2\pi \frac{\alpha^2 v}{s} \left[1 + \frac{(1 - v^2)}{2} - \frac{(3 - 2v^2 - v^4)}{4v} \ln \frac{1+v}{1-v} \right] \quad (10)$$

The full differential Born cross-section is found to be

$$\frac{d\sigma_B(\gamma\gamma \rightarrow \pi^+\pi^-)}{d\Omega} = \frac{\alpha^2 v}{2s} \left[\left(1 - \frac{v^2 \sin^2 \theta}{1 - v^2 \cos^2 \theta} \right)^2 + \frac{(v^2 \sin^2 \theta)^2}{(1 - v^2 \cos^2 \theta)^2} \right] \quad (11)$$

and integrating over the full angular range yields the Born cross-section

$$\sigma_B(\gamma\gamma \rightarrow \pi^+\pi^-) = 2\pi \frac{\alpha^2 v}{s} \left[2 - v^2 - \frac{1 - v^4}{2v} \ln \frac{1+v}{1-v} \right] \quad (12)$$

in agreement with the result of [37].

B. Non-perturbative strong-interaction contributions to the meson-meson reaction amplitudes

To obtain the full transition matrix shown in Fig. 1a), the effects of the strong interaction in the final state must now be taken into account. In particular, we first need to evaluate the T -matrices that are associated with the square diagram in Fig. 1a) and which account for meson-meson scattering. Here we follow the approach offered by CHPT, following [34] and briefly summarizing the essential points. The meson pairs $(K\bar{K})^I$, $(\pi\pi)^I$ and $(\pi^0\eta)^I$ of good isospin I , interact in the final state via 4-point vertices given by [35] [44]

$$V_{m_1 m_2; m_3 m_4}^I = \langle I, m_1 m_2 | \mathcal{L}_2 | I, m_3 m_4 \rangle = V_{m_3 m_4; m_1 m_2}^I$$

$$\mathcal{L}_2 = \frac{1}{12f^2} \text{Tr}_f \left((\partial_\mu \Phi \Phi - \Phi \partial_\mu \Phi)^2 + M \Phi^4 \right), \quad (13)$$

at tree level, after coupling both the initial and final two-meson states to good isospin I . The symmetry in the interaction under the interchange of labels is due to time-reversal invariance. \mathcal{L}_2 is the leading order CHPT interaction Lagrangian density [32, 33]; Tr_f denotes the trace in $SU(3)$ flavor space of the matrices constructed from

$$\Phi = \begin{pmatrix} \frac{1}{\sqrt{2}}\pi^0 + \frac{1}{\sqrt{6}}\eta & \pi^+ & K^+ \\ \pi^- & -\frac{1}{\sqrt{2}}\pi^0 + \frac{1}{\sqrt{6}}\eta & K^0 \\ K^- & \bar{K}^0 & -\frac{2}{\sqrt{6}}\eta \end{pmatrix};$$

In (13), $M = \text{diag}(m_\pi^2, m_\pi^2, 2m_K^2 - m_\pi^2)$ is a diagonal matrix of (bare) meson masses, and f is the (bare) pion decay constant.

Notationally, we abbreviate the 4-point vertices in (13) and the meson-meson transition amplitudes $T_{m_1 m_2 \rightarrow m_3 m_4}$ in a compact fashion as has been previously introduced in [34]. The indices $(i, j) = (1, 2)$ are used to identify the specific meson *pair* involved: 1 indicates $K\bar{K}$ in both isospin states $I = 0$ and 1, while 2 indicates $\pi\pi$ for $I = 0$ (or $I = 2$), and $\pi^0\eta$ for $I = 1$, see (A.11) through (A.15) in the Appendix. (Note that this follows the convention of [35], but is *opposite* to the channel labelling convention of [14]). Using the V_{ij}^I obtained from (13), one constructs the coupled equations for the scattering amplitudes T_{ij}^I of good isospin for these meson pairs. In general these

are integral equations that involve meson–meson interactions V_{ij}^I in intermediate states, where at least one of the states i or j is off-shell. However, in the case of s -wave scattering, Oller and Oset have shown explicitly [34] that one can replace the V_{ij}^I by their on-shell values in intermediate states too, since their off-shell parts are additive and can be re-absorbed as a renormalization factor that replaces the “bare” coupling constant $1/f$ and meson masses by their physical values, $f_\pi \approx 93$ MeV and $(m_\pi, m_K, m_\eta) \approx (140, 496, 547)$ MeV.

The on-shell versions of V_{ij}^I are listed explicitly in (A.16). These only depend on the external variable $s = P_0^2$, the total center-of-mass energy squared of the meson pair. This in turn means that the integration over the four-momenta of meson pairs in intermediate states can be factored [34], and the coupled integral equations for the $T_{ij}^I(s)$ become coupled algebraic equations that can be solved exactly. The results are

$$T_{11}^I(s) = [(1 - V_{22}^I \Pi_{22}^I) V_{11}^I + V_{12}^I \Pi_{22}^I V_{21}^I] [D^I(s)]^{-1} \quad (14)$$

$$T_{12}^I(s) = V_{12}^I [D^I(s)]^{-1} \quad (15)$$

for $(K\bar{K})^I \rightarrow (K\bar{K})^I$ in both isospin channels, $I = 0, 1$, and $(K\bar{K})^0 \rightarrow (\pi\pi)^0$ or $(K\bar{K})^1 \rightarrow (\pi^0\eta)^1$ respectively. Notice that $T_{12}^I(s) = T_{21}^I(s)$ is also time-reversal invariant. In the equations (14) and (15), Π_{ii}^I denotes the meson loop diagrams and is given by

$$\frac{1}{i} \Pi_{ii}^I(s) = -\epsilon \int \frac{d^4 l}{(2\pi)^4} \frac{1}{(l^2 - m_a^2)} \frac{1}{(l + P_0)^2 - m_b^2}, \quad s = P_0^2 \quad (16)$$

for two mesons of mass (m_a, m_b) as identified by the labels I and i ; the symmetry factor $\epsilon = [1/2, 1]$ for identical (non-identical) mesons propagating in the loop [39]. Thus $\Pi_{11}^I = \Pi_{K\bar{K}}$ for $K\bar{K}$ in both isospin channels, while $\Pi_{22}^I = \Pi_{\pi\pi}$ for $I = (0, 2)$ or $\Pi_{\pi^0\eta}$ for $I = 1$. The common denominator of $T_{11}^I(s)$ and $T_{12}^I(s)$, $D^I(s)$, is given by

$$D^I(s) = (1 - V_{11}^I \Pi_{11}^I)(1 - V_{22}^I \Pi_{22}^I) - V_{12}^I \Pi_{22}^I V_{21}^I \Pi_{11}^I, \quad I = (0, 1) \quad (17)$$

Since pions coupled to good isospin behave like identical bosons [39], $(\pi\pi)^I \rightarrow (\pi\pi)^I$ s -wave scattering can only occur for $I = 0$ or 2 . The relevant T -matrices are

$$T_{22}^0(s) = [T_{11}^0(s)]_{1 \leftrightarrow 2} \quad (18)$$

$$T_{22}^2(s) = V_{22}^2 (1 - V_{22}^2 \Pi_{22}^2)^{-1} \quad (19)$$

for $(\pi\pi)^0 \rightarrow (\pi\pi)^0$ and $(\pi\pi)^2 \rightarrow (\pi\pi)^2$, since in the latter channel only the diagonal interaction vertex V_{22}^2 is non-zero, see (A.16). The related S matrix element, $S_{22}^2 = \exp(2i\delta_2^2)$, where δ_2^2 is a real phase shift, is thus unitary.

The integral in (16) diverges at large four-momenta and requires regularization. Explicit expressions for the loop integrals (with and without differing masses) are given in [31] using a cut-off Λ in $O(4)$ momentum space, see (A.17) to (A.19). Thus, the $T_{ij}^I(s)$ are all known in closed form.

The complex poles in $P_0 = \sqrt{s}$ of the transition amplitudes $T_{11}^I(P_0)$ and $T_{12}^I(P_0)$ in (14) and (15) can be found for $I = (0, 1)$ from the roots of their common denominator $D^I(P_0^2) = 0$ in (17). These roots, which determine the meson mass M^I and half-width $\Gamma^I/2$ for each isospin, lie on the appropriate second sheet [34] in the lower half of the cut complex P_0 -plane, i.e. $P_0^I = (M^I - \frac{i}{2}\Gamma^I)$. This relation assumes a non-relativistic Breit–Wigner shape for the transition amplitude in the vicinity of its peak value at $P_0 = M^I$.

One finds two roots for $I = 0$ and a single root for $I = 1$, that correspond to the two scalar-isoscalar mesons $f_0(500)$ (or σ), $f_0(980)$ and a single scalar-isovector $a_0(980)$ meson respectively [35]. We use the $O(4)$ cutoff of $\Lambda = 1.351_{+0.160}^{-0.185}$ GeV that fixes [31] the real part of one $I = 0$ root,

TABLE I: Summary of calculated masses and half-widths, $M^I - \frac{i}{2}\Gamma^I$ (in MeV, rounded to the nearest integer) for $f_0(500)$ or σ , $f_0(980)$ and $a_0(980)$ as a function of the range of $O(4)$ cutoff Λ 's = $1.351_{+0.160}^{-0.185}$ GeV. The other input parameters are taken from experiment: $f_\pi = 93$ MeV and $(m_\pi, m_K, m_\eta) = (140, 496, 547)$ MeV.

Λ GeV	$M_\sigma^0 - \frac{i}{2}\Gamma_\sigma^0$	$M_{f_0}^0 - \frac{i}{2}\Gamma_{f_0}^0$	$M_{a_0}^1 - \frac{i}{2}\Gamma_{a_0}^1$
1.166	$466 - 201i$	$990 - 16i$	$987 - 52i$
1.351	$474 - 192i$	$980 - 23i$	$964 - 53i$
1.511	$479 - 186i$	$970 - 28i$	$946 - 52i$
PDG[40]	$(400 - 1200) - (300 - 500)i$	$(980 \pm 10) - (25 - 50)i$	$(980 \pm 20) - (20 - 50)i$
PDG[40]	$(400 - 550) - (200 - 350)i$	$(990 \pm 20) - (20 - 50)i$	$(980 \pm 20) - (25 - 50)i$

with error bars, at $M_{f_0}^0 = (980 \pm 10)$ MeV. This replicates the $f_0(980)$ mass values quoted in the PDG data table [40]. The predictions for the masses and half-widths for all three scalar mesons are listed in Table I.

We are now able to construct the contribution in which the strong interaction influences the final state. According to the second diagram in Fig. 1 (a) we identify $T_{S;\gamma\gamma \rightarrow m_1 m_2}^{\mu\nu}$ to be given by the gauge invariant expression

$$\begin{aligned}
T_{S;\gamma\gamma \rightarrow m_1 m_2}^{\mu\nu} &= T(s)_{m_1 m_2; m_+ m_-} \left\{ \int \frac{d^4 l}{(2\pi)^4} \frac{1}{i} \Delta(q_1 + l) \frac{1}{i} \Delta(q_2 - l) < q_1 + l, q_2 - l | iT_B^{\mu\nu} | q_1 q_2 > \right\} \\
&\approx -\frac{e^2}{2\pi^2} [g^{\mu\nu} (q_1 \cdot q_2) - q_2^\mu q_1^\nu] \frac{J_{m_\pm}(s)}{2s} T(s)_{m_1 m_2; m_+ m_-}
\end{aligned} \tag{20}$$

for a propagating charged meson pair $m_+ m_-$ in the loop. In (20), Δ is the meson propagator $\Delta(p) = 1/(p^2 - m_\pm^2 + i0^+)$, with m_\pm being the charged meson mass m_π or m_K , as appropriate. $T_{m_1 m_2; m_+ m_-}$ is the meson-meson scattering contribution which is constructed from (14) - (19) for the appropriate meson pairs. The function $J_{m_\pm}(s)$ is found to be

$$\begin{aligned}
J_{m_\pm}(s) &= \left\{ 1 - \frac{4m_\pm^2}{s} \left[\sin^{-1} \sqrt{\frac{s}{4m_\pm^2}} \right]^2 \right\} \theta(4m_\pm^2 - s) \\
&\quad + \left\{ 1 + \frac{4m_\pm^2}{s} \left[\cosh^{-1} \sqrt{\frac{s}{4m_\pm^2}} - i\frac{\pi}{2} \right]^2 \right\} \theta(s - 4m_\pm^2).
\end{aligned}$$

In this expression, the second term for $s \geq 4m_\pm^2$ arises by continuing the first as a function of s onto the upper lip of the cut $4m_\pm^2 < s < \infty$ along the real axis of the complex s -plane.

The final result in (20) follows after factoring out the meson-meson scattering box diagram from the integral. This approximation [35], like that for $T_{ij}^I(s)$, places the intermediate incoming charged meson pair $m_+ m_-$ of $T_{m_1 m_2; m_+ m_-}$ on-shell to render this amplitude a function of s only. Note, however, that the charged mesons in the final state of $iT_B^{\mu\nu}$ under the integral sign are, by contrast, both still off-shell. Allowing for different combinations of intermediate meson pairs to be

formed, the contribution from the final-state strong interactions to the full (contracted) T matrix thus reads

$$T_{S;\gamma\gamma\rightarrow m_1 m_2} = (\epsilon_{1\mu} T_{S;\gamma\gamma\rightarrow m_1 m_2}^{\mu\nu} \epsilon_{2\nu}) = -\frac{e^2}{8\pi^2} (\epsilon_1 \cdot \epsilon_2) \sum_{m_{\pm}} J_{m_{\pm}}(s) T(s)_{m_1 m_2; m_+ m_-}. \quad (21)$$

This scattering amplitude is independent of the scattering angle and is thus pure s -wave. Hence

$$T_{S;\gamma\gamma\rightarrow m_1 m_2}^{(0,0)} = \frac{ie^2}{8\pi^2} \left[\sum_{m_{\pm}} J_{m_{\pm}}(s) T_{m_1 m_2; m_+ m_-} \right] \sqrt{4\pi} Y_{0,0} \quad (22)$$

when contracted with respect to polarization vectors of total helicity $\lambda = 0$. There is no $\lambda = 2$ contribution in this case.

C. Non-Chiral Perturbation Theory contributions

As already commented upon in the Introduction, additional s -channel background contributions $T_{R;\gamma\gamma\rightarrow m_1 m_2}^{(2,2)}$ from the $f_2(1270)$ and $a_2(1320)$ resonances with quantum numbers $I^G(J^{PC}) = 0^+(2^{++})$ and $1^-(2^{++})$ to the scattering amplitude can be expected to be important at center-of-mass energies below 1 GeV. We denote these as $T_{R;\gamma\gamma\rightarrow m_1 m_2}^{(2,2)}$. In addition, the t -channel axial exchange amplitude arising from the $1^-(1^{++})$ $a_1(1260)$ resonance, denoted as $T_{A;\gamma\gamma\rightarrow\pi^0\eta}$, also not only plays a role above $\sim \mathcal{O}(1 \text{ GeV})$ [35, 37], but also influences the amplitudes and cross-sections below 1 GeV. All such contributions lie beyond the scope of the CHPT calculations outlined above and are parametrized.

The f_2 and a_2 resonances have been interpreted [36] as pure d -wave, helicity 2 states $(J, \lambda) = (2, 2)$. We parametrize these by a relativistic Breit-Wigner resonance amplitude [41] for $\gamma\gamma \rightarrow M_R \rightarrow m_1 m_2$ as

$$T_{R;\gamma\gamma\rightarrow m_1 m_2}^{(2,2)} = -16\pi \sqrt{\frac{20\pi}{v}} [\Gamma_{\gamma\gamma}^{(2)}]^{1/2} \frac{i\sqrt{s}}{s - M_R^2 + iM_R\Gamma} [Br(m_1 m_2)\Gamma]^{1/2} Y_{2,2}(\theta, \phi), \quad R = f_2, a_2 \quad (23)$$

for a resonance of mass and total width M_R, Γ respectively and with partial widths $\Gamma_{\gamma\gamma}^{(2)}$ and $\Gamma(m_1 m_2) = Br(m_1 m_2)\Gamma$ for the decay into two photons of opposite helicity, or two mesons respectively; $Br(m_1 m_2)$ is the branching ratio for the latter decay.

Due to their large total widths (~ 100 to 200 MeV), the a_2 and f_2 resonances can contribute to production cross sections already at energies $\sim 1 \text{ GeV}$, well below their peak positions. We will illustrate this in the next section for the $\gamma\gamma \rightarrow \pi^0\pi^0$ channel where the total cross-section, (26), is just the sum of the partial cross-sections determined by CHPT and the f_2 resonance amplitudes separately, without any interference term.

D. Total $\gamma\gamma \rightarrow$ meson-meson transition amplitudes and cross-sections

The total contracted transition amplitudes $T_{\gamma\gamma\rightarrow m_1 m_2}$ can now be calculated from (1). For each specific exit channel, this can be written to leading order as a sum of s - and d -wave components:

$$T_{\gamma\gamma\rightarrow m_1 m_2} = T_{\gamma\gamma\rightarrow m_1 m_2}^{(0,0)} + T_{\gamma\gamma\rightarrow m_1 m_2}^{(2,2)}, \quad (24)$$

where

$$T_{\gamma\gamma \rightarrow m_1 m_2}^{(J,\lambda)} = T_{B;\gamma\gamma \rightarrow m_1 m_2}^{(J,\lambda)} + T_{S;\gamma\gamma \rightarrow m_1 m_2}^{(J,\lambda)} + T_{R(A);\gamma\gamma \rightarrow m_1 m_2}^{(J,\lambda)}, \quad (25)$$

and the relevant components are selected for the Born term and the strong interaction term (from CHPT), while resonant or axial terms (non-CHPT) are taken from (7), (22) and (23), as appropriate. The total $\gamma\gamma \rightarrow$ meson-meson cross-section can then be expressed as the sum of the moduli squared of the $T^{(J,\lambda)}$, due to the orthogonality of the spherical harmonics they contain. One has

$$\begin{aligned} \sigma(\gamma\gamma \rightarrow m_1 m_2) &= \frac{1}{2} \frac{v}{64\pi^2 s} \epsilon \int d\Omega |T_{\gamma\gamma \rightarrow m_1 m_2}|^2 = \frac{1}{2} \frac{v}{64\pi^2 s} \epsilon \int d\Omega \left[|T_{\gamma\gamma \rightarrow m_1 m_2}^{(0,0)}|^2 + |T_{\gamma\gamma \rightarrow m_1 m_2}^{(2,2)}|^2 \right] \\ &= \sigma^{(0,0)}(\gamma\gamma \rightarrow m_1 m_2) + \sigma^{(2,2)}(\gamma\gamma \rightarrow m_1 m_2) \end{aligned} \quad (26)$$

after integrating over the full solid angle and averaging over the two helicities of the incoming photon pair. The individual $T_{\gamma\gamma \rightarrow m_1 m_2}$ matrices $T_{\gamma\gamma \rightarrow m_1 m_2}^{(0,0)}$ and $T_{\gamma\gamma \rightarrow m_1 m_2}^{(2,2)}$ that determine these partial cross sections are given explicitly in Table II for the three exit channels $m_1 m_2 = \pi^0 \pi^0$, $\pi^+ \pi^-$ and $\pi^0 \eta$.

TABLE II: Combinations of partial T -matrices of good angular momentum and helicity (J, λ) that determine $|T_{\gamma\gamma \rightarrow m_1 m_2}|^2$ in Eq. (26) for the production cross-section of a meson pair, $\gamma\gamma \rightarrow m_1 m_2$. The contributions to the T -matrices incorporating the additional resonant and t -channel axial exchange contributions not generated by the CHPT Lagrangian are labelled explicitly by the resonance or axial term that characterizes them.

$m_1 m_2$	ϵ	$v = p/q$	$ T_{\gamma\gamma \rightarrow m_1 m_2} ^2 = T_{\gamma\gamma \rightarrow m_1 m_2}^{(0,0)} ^2 + T_{\gamma\gamma \rightarrow m_1 m_2}^{(2,2)} ^2$
$\pi^0 \pi^0$	1/2	$\left[1 - \frac{4m_\pi^2}{s}\right]^{1/2}$	$ T_{S,\gamma\gamma \rightarrow \pi^0 \pi^0}^{(0,0)} ^2 + T_{f_2;\gamma\gamma \rightarrow \pi^0 \pi^0}^{(2,2)} ^2$
$\pi^+ \pi^-$	1	$\left[1 - \frac{4m_\pi^2}{s}\right]^{1/2}$	$ T_{B,\gamma\gamma \rightarrow \pi^+ \pi^-}^{(0,0)} + T_{S,\gamma\gamma \rightarrow \pi^+ \pi^-}^{(0,0)} ^2 + T_{B,\gamma\gamma \rightarrow \pi^+ \pi^-}^{(2,2)} + \mathcal{T}_{f_2;\gamma\gamma \rightarrow \pi^+ \pi^-}^{(2,2)} ^2$
$\pi^0 \eta$	1	$\left[1 - \frac{(m_\pi - m_\eta)^2}{s}\right]^{1/2} \left[1 - \frac{(m_\pi + m_\eta)^2}{s}\right]^{1/2}$	$ T_{S,\gamma\gamma \rightarrow \pi^0 \eta}^{(0,0)} + T_{A;\gamma\gamma \rightarrow \pi^0 \eta}^{(0,0)} ^2 + T_{a_2;\gamma\gamma \rightarrow \pi^0 \eta}^{(2,2)} ^2$

III. NUMERICAL RESULTS FOR SCATTERING AMPLITUDES AND CROSS-SECTIONS

A. $m_1 m_2 \rightarrow m_3 m_4$ scattering amplitudes

One of the main contributions to the total scattering amplitude in (1) arises from final-state strong interactions through meson-meson scattering. The latter amplitudes themselves are an important input to the photon-photon cross-sections, and were calculated separately in Section IIB within the framework of CHPT. In [14] these amplitudes have been extracted from the data in a model-independent fashion. Here we compare our calculated results for the real and imaginary parts of the transition matrices with the results of their fits, see Fig. 2, for the processes $\pi\pi \rightarrow \pi\pi$, $\pi\pi \rightarrow K\bar{K}$ and $K\bar{K} \rightarrow K\bar{K}$.

As can be seen in this figure, there is an overall good qualitative agreement between the transition matrices calculated from CHPT and those extracted from experiment. However, quantitatively

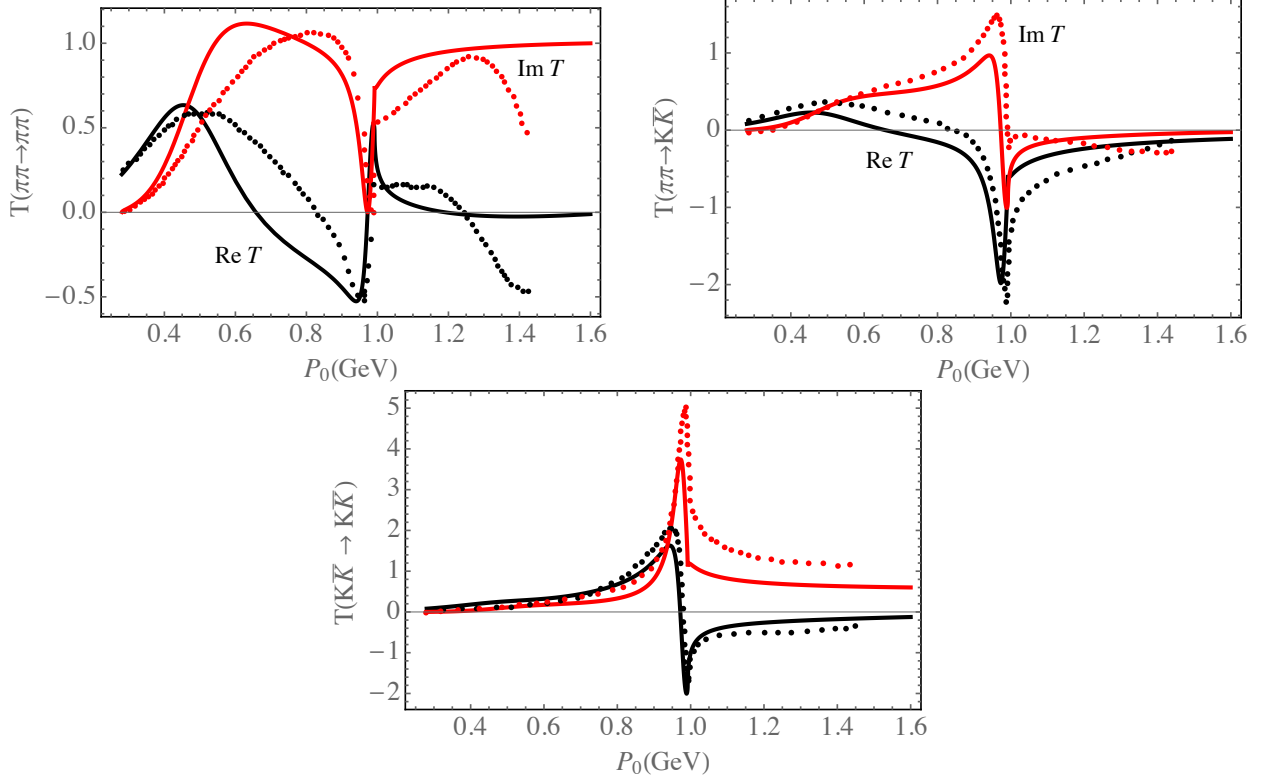


FIG. 2: (Color online) The T -matrix elements for the meson-meson scattering amplitudes $\pi\pi \rightarrow \pi\pi$, $\pi\pi \rightarrow K\bar{K}$ and $K\bar{K} \rightarrow K\bar{K}$. The solid curves are this calculation, the dotted curves are the values extracted from the data by Dai and Pennington [14]. The real parts are given by the black curves, the imaginary values by the red ones.

there are differences, notably for the transition $\pi\pi \rightarrow \pi\pi$, in which the real part underestimates the extracted values at energies below 1.0 GeV, while the imaginary part overestimates the extracted values in the lower energy range, peaking at a lower value of P_0 .

Having determined these amplitudes, we focus on the photon-photon to meson-meson cross-sections.

B. $\gamma\gamma \rightarrow m_1 m_2$ cross-sections

1. $\gamma\gamma \rightarrow \pi^0 \pi^0$ cross-sections

The cross-section $\gamma\gamma \rightarrow \pi^0 \pi^0$ is often considered to be particularly instructive, as it lacks a Born term. Thus, the contributions from the a_2 and f_2 (as well as the possibilities that could arise from new physics) can be investigated more closely. Due to the large total widths of these two resonances (~ 100 to 200 MeV respectively), they can be expected to contribute to production cross-sections already at energies ~ 1 GeV, well below their peak positions. In the $\gamma\gamma \rightarrow \pi^0 \pi^0$ channel the total cross-section given in (26) is just the sum of the partial cross-sections determined by CHPT and f_2 resonance amplitudes separately, without any interference term, as seen in Table II. The results are shown in Fig. 3 where the calculated total cross-section as well as the pure $(J, \lambda) = (0, 0)$ chiral contribution are compared with the recent Belle [2] as well as the older Crystal Ball Collaboration [5, 6] data. The transition amplitudes for these calculations come from (22) and (23) for $T_{S; \gamma\gamma \rightarrow \pi^0 \pi^0}^{(0,0)}$

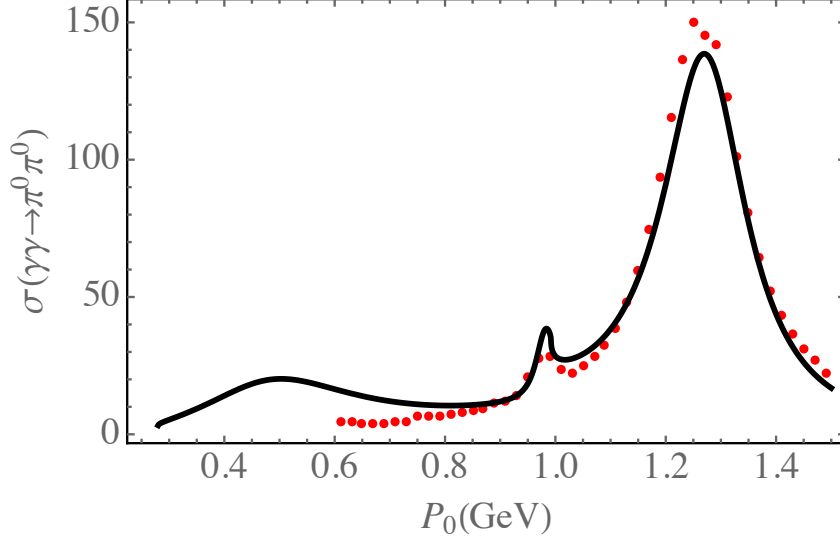


FIG. 3: (Color online) Cross-section for $\gamma\gamma \rightarrow \pi\pi$ integrated over the restricted angular range $\cos\theta < 0.6$ (solid black curve) compared to the data of the Belle [2], Crystal Ball and JADE Collaborations [5, 6] (red dots).

and $T_{f_2; \gamma\gamma \rightarrow \pi^0\pi^0}^{(2,2)}$ evaluated at cutoff $\Lambda = 1.351$ GeV in the first case, and using a mass, total width, and branching ratio of $(M_{f_2}, \Gamma_{f_2}) = (1275, 185)$ MeV and $[\Gamma_{\gamma\gamma}^{(2)} Br(\pi^0\pi^0) \Gamma_{f_2}] = 0.16$ MeV² for the second resonance amplitude as extracted from the PDG tables [40].

One notes that the CHPT cross-section is lifted up sufficiently in the vicinity of ~ 1 GeV by the low energy tail of the $f_2(1275)$ resonance contribution to lead to an acceptable overall fit with experiment. This result in turn confirms that the chiral $(0,0)$ cross-section is correct for center-of-mass energies below ~ 1 GeV.

The cross-section for $\gamma\gamma \rightarrow \pi\pi$ integrated over the full angular range is shown in Fig. 4. Here one sees again that the resonance f_2 underestimates the results of Dai and Pennington in its strength, and some discrepancy is also observed at lower energies.

In Fig. 5 we show the results for the process $\gamma\gamma \rightarrow \pi^+\pi^-$. In this figure, the dotted curve represents the extracted data of Dai and Pennington [14], integrated over the full angular range. The blue dashed curve is our calculation, without including the effects of the final-state strong interactions, while the black solid curve indicates our final full calculation, including the final-state strong interactions. As expected, the Born contribution to this process plays a dominant role at low energies. After 0.9 GeV, this calculation is in very good agreement with the extracted data.

IV. SUMMARY AND CONCLUSIONS

In this paper, we have calculated the amplitudes and cross-sections for light-light collisions giving rise to $\pi^+\pi^-$, $\pi^0\pi^0$ and $K\bar{K}$ in the final state. Our theoretical framework combines the Born scattering transition amplitudes required through QED with those that can be calculated via CHPT to describe the low-energy regime, and includes parametrizations of the resonant mesons such as $f_2(1279)$ and $a_2(1302)$, which cannot be accounted for within CHPT, but which are essential for the evaluation of the cross-sections. We compare our results with those extracted from [14] which are extracted from all the data available today, including the high statistics data from Belle, as well as the older data from Mark II at SLAC, CELLO at DESY and the Crystal Ball at SLAC

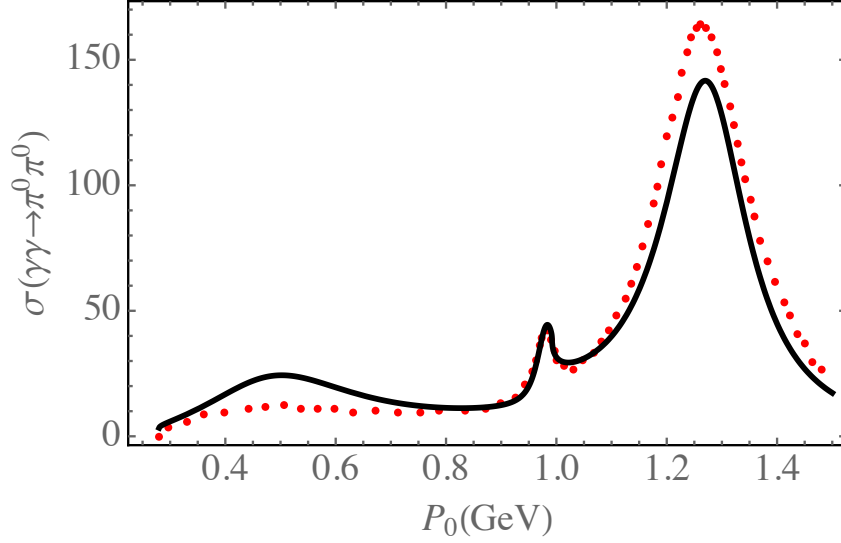


FIG. 4: (Color online) Cross-section for $\gamma\gamma \rightarrow \pi\pi$ integrated over the full angular range (solid black curve) compared to the extracted curve denoted as Sol I of Dai and Pennington [14] (red dots) .

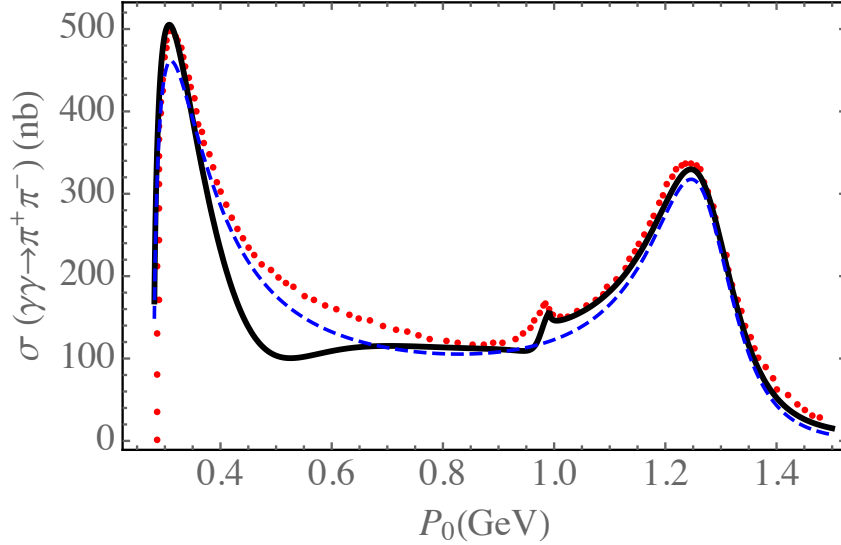


FIG. 5: (Color online) Cross-section for $\gamma\gamma \rightarrow \pi^+\pi^-$ integrated over the full angular range (solid black curve) compared to the extracted curve denoted as Sol I of Dai and Pennington [14] (red dots). The blue dashed curve is a calculation not including the effects of the strong interaction.

and fitted using basic constraints of analyticity, unitarity and crossing symmetry, as well as Low's low-energy theorem for QED. It is interesting that they are not only able to fit the cross-sections, but also able to obtain the strong-interaction transition matrices, to which we have been able to compare our theoretical model. The results of the comparison are reasonable, showing all expected structures, but they are not perfect.

It remains an intriguing question as to whether new structures, such as the postulated existence of the kaonic atom K^+K^- actually exists and can be observed. This will be addressed elsewhere.

V. ACKNOWLEDGMENTS

One of us (SPK) thanks NITheP for financial support and the University of the Witwatersrand for its kind hospitality. This paper is dedicated to R.H. Lemmer, who passed away during the preparation of the manuscript and whose presence is sadly missed.

Appendix

Born term helicity amplitudes

Writing (3) in the center-of-mass system and using polarization vectors in the helicity representation one finds [35]

$$\begin{aligned} T_{B;\gamma\gamma\rightarrow m^+m^-}^{(0)} &= -2e^2 i \left\{ 1 - \frac{v^2 \sin^2 \theta}{1 - \mathbf{v}^2 \cos^2 \theta} \right\} = -\frac{2ie^2(1-v^2)}{1 - \mathbf{v}^2 \cos^2 \theta} \\ &= -2ie^2 \sum_{J=0,2,\dots} \sqrt{4\pi}(2J+1)^{1/2} \frac{1-v^2}{v} Q_J(1/v) Y_{J,0}(\theta, \phi), \quad 1/v > 1 \end{aligned} \quad (\text{A.1})$$

when expanded in terms of spherical harmonics $Y_{J,\lambda}(\theta, \phi)$. Here $Q_J(1/v)$ is a Legendre function of the second kind [42]. The (J, λ) partial wave amplitude for helicity zero is thus identified as

$$T_{B;\gamma\gamma\rightarrow m^+m^-}^{(J,0)} = -2ie^2 \sqrt{4\pi}(2J+1)^{1/2} \frac{1-v^2}{v} Q_J(1/v) Y_{J,0}(\theta, \phi). \quad J = 0, 2, 4, \dots \quad (\text{A.2})$$

Setting $J = 0$ and using $Q_0(1/v) = \frac{1}{2} \ln [(1+v)/(1-v)]$ one recovers $T_{B;\gamma\gamma\rightarrow m^+m^-}^{(0,0)}$ of (7).

Likewise

$$\begin{aligned} T_{B;\gamma\gamma\rightarrow m^+m^-}^{(2)} &= \frac{2ie^2 v^2 \sin^2 \theta e^{2i\phi}}{1 - v^2 \cos^2 \theta} = \frac{2ie^2 v^2}{1 - v^2 \cos^2 \theta} \sqrt{\frac{32\pi}{15}} Y_{2,2}(\theta, \phi) \\ &= 2ie^2 v^2 \sqrt{\frac{32\pi}{15}} \sum_{l=0,2,\dots} \sqrt{4\pi}(2l+1)^{1/2} \frac{1}{v} Q_l(1/v) Y_{l,0}(\theta, \phi) Y_{2,2}(\theta, \phi) \end{aligned} \quad (\text{A.3})$$

We now make use of the expression for the product of the two spherical harmonics $Y_{l,0}(\theta, \phi) Y_{2,2}(\theta, \phi)$ at a common angle [43] to find

$$\begin{aligned} T_{B;\gamma\gamma\rightarrow m^+m^-}^{(2)} &= 2ie^2 v^2 \left(\frac{32\pi}{3}\right)^{1/2} \frac{1}{v} \sum_{J=2,4,\dots} (2J+1)^{1/2} \\ &\quad \times \left\{ \sum_{l=J-2, J, J+2} (2l+1) \begin{pmatrix} l & 2 & J \\ 0 & 2 & -2 \end{pmatrix} \begin{pmatrix} l & 2 & J \\ 0 & 0 & 0 \end{pmatrix} Q_l(1/v) \right\} Y_{J,2}(\theta, \phi). \end{aligned} \quad (\text{A.4})$$

The restriction on the sum over l is due to the second Wigner $3-j$ symbol [43] that vanishes unless $l+2+J$ is even. Inserting their specific values given in [43] one can perform the l -sum in the curly brackets to identify the $(J, 2)$ partial-wave amplitude as

$$\begin{aligned}
T_B^{(J,2)} = & 2ie^2\sqrt{4\pi}(2J+1)^{1/2}\left\{[(J-1)J(J+1)(J+2)]^{1/2}v\right. \\
& \times\left(\frac{Q_{J-2}(1/v)}{(2J-1)(2J+1)} - 2\frac{Q_J(1/v)}{(2J-1)(2J+3)} + \frac{Q_{J+2}(1/v)}{(2J+1)(2J+3)}\right)\Big\}Y_{J,2}(\theta, \phi), \\
& J = 2, 4, 6, \dots
\end{aligned} \tag{A.5}$$

For $J = 2$ the value of the expression in curly brackets reduces to

$$\begin{aligned}
\left\{\dots\right\} &= (24)^{1/2}v\left[\frac{1}{15}Q_0(1/v) - \frac{2}{21}Q_2(1/v) + \frac{1}{35}Q_4(1/v)\right] \\
&= \frac{1}{2}\sqrt{\frac{3}{2}}\left[-\frac{1}{v^2} + \frac{5}{3} + \frac{(1-v^2)^2}{2v^3}\ln\frac{1+v}{1-v}\right]
\end{aligned} \tag{A.6}$$

Substituting this result back into Eq. (A.5) leads to the value of the $(2, 2)$ Born helicity amplitude quoted in (7) of the main text.

We also record the total Born cross-sections for given helicity as determined by $T_B^{(0,0)}$, $T_B^{(2,2)}$ as well as those determined by $T_B^{(0)}$, $T_B^{(2)}$ respectively,

$$\sigma_B^{(0,0)}(\gamma\gamma \rightarrow \pi^+\pi^-) = 2\pi\frac{\alpha^2v}{s}\left[\frac{1-v^2}{2v}\ln\frac{1+v}{1-v}\right]^2 \tag{A.7}$$

$$\sigma_B^{(2,2)}(\gamma\gamma \rightarrow \pi^+\pi^-) = 2\pi\frac{\alpha^2v}{s}\left[-\frac{1}{v^2} + \frac{5}{3} + \frac{(1-v^2)^2}{2v^3}\ln\frac{1+v}{1-v}\right]^2\left(\frac{15}{8}\right) \tag{A.8}$$

$$\sigma_B^{(0)}(\gamma\gamma \rightarrow \pi^+\pi^-) = 2\pi\frac{\alpha^2v}{s}\left[\frac{(1-v^2)}{2} + \frac{(1-v^2)^2}{4v}\ln\frac{1+v}{1-v}\right] \tag{A.9}$$

$$\sigma_B^{(2)}(\gamma\gamma \rightarrow \pi^+\pi^-) = 2\pi\frac{\alpha^2v}{s}\left[1 + \frac{(1-v^2)}{2} - \frac{(3-2v^2-v^4)}{4v}\ln\frac{1+v}{1-v}\right] \tag{A.10}$$

On-shell interaction vertices of good isospin

The following set of basis states of good isospin I , $|(M_1M_2)^I\rangle$, are defined in terms of the meson-meson particle basis set to be:

$$|(K\bar{K})^{0,1}\rangle = -\frac{1}{\sqrt{2}}[K^+K^- \pm K^0\bar{K}^0] \tag{A.11}$$

$$|(\pi\pi)^0\rangle = -\frac{1}{\sqrt{3}}[\pi^+\pi^- + \pi^-\pi^+ + \pi^0\pi^0], \tag{A.12}$$

$$|(\pi\pi)^1\rangle = -\frac{1}{\sqrt{2}}[\pi^+\pi^- - \pi^-\pi^+] \tag{A.13}$$

$$|(\pi\pi)^2\rangle = -\frac{1}{\sqrt{6}}[\pi^+\pi^- + \pi^-\pi^+ - 2\pi^0\pi^0] \tag{A.14}$$

$$|(\pi^0\eta)^1\rangle = \pi^0\eta \tag{A.15}$$

The on-shell values [45] for the V_{ij}^I can then be found from the information given in [34] to be

$$\begin{aligned} V_{11}^0 &= \frac{3}{4} \frac{s}{f^2}, & V_{21}^0 &= \frac{1}{2} \sqrt{\frac{3}{2}} \frac{s}{f^2}, & V_{22}^0 &= \frac{1}{f^2} (2s - m_\pi^2) \\ V_{11}^1 &= \frac{1}{4} \frac{s}{f^2}, & V_{21}^1 &= -\sqrt{\frac{2}{3}} \frac{1}{f^2} \left(\frac{3}{4} s - \frac{1}{12} m_\pi^2 - \frac{1}{4} m_\eta^2 - \frac{2}{3} m_K^2 \right), & V_{22}^1 &= \frac{1}{3} \frac{m_\pi^2}{f^2} \\ V_{22}^2 &= -\frac{1}{f^2} (s - 2m_\pi^2) \end{aligned} \quad (\text{A.16})$$

Here \sqrt{s} is the total collisional energy in the center-of-mass system.

Meson loop integrals

The expression [31] for the $O(4)$ regularized integral $\Pi_{ii}^I(s) = \Pi(s)$ in Eq. (16) depends on where s lies relative to the cut that starts at the branch point $(m_a + m_b)^2$. For $s > (m_a + m_b)^2$ on the upper lip of the cut along the real axis, the integral acquires an imaginary part and one finds

$$\Pi(s) = \frac{\epsilon}{(4\pi)^2} \left[\frac{m_a^2}{m_a^2 - m_b^2} \ln\left(1 + \frac{\Lambda^2}{m_a^2}\right) - \frac{m_b^2}{m_a^2 - m_b^2} \ln\left(1 + \frac{\Lambda^2}{m_b^2}\right) - L_{ab}(s) \right] \quad (\text{A.17})$$

with $L_{ab}(s)$ given by

$$\begin{aligned} L_{ab}(s) &= -1 - \frac{1}{2} \left(\frac{m_a^2 + m_b^2}{m_a^2 - m_b^2} - \frac{m_a^2 - m_b^2}{s} \right) \ln \frac{m_a^2}{m_b^2} \\ &\quad + \sqrt{f_{ab}} \left[\tanh^{-1} \left(\frac{\sqrt{f_{ab}}}{1 - \frac{m_a^2 - m_b^2}{s}} \right) + \tanh^{-1} \left(\frac{\sqrt{f_{ab}}}{1 + \frac{m_a^2 - m_b^2}{s}} \right) \right] - i\pi \sqrt{f_{ab}}, \quad s > (m_a + m_b)^2 \\ \sqrt{f_{ab}} &= \left(1 - \frac{(m_a - m_b)^2}{s} \right)^{1/2} \left(1 - \frac{(m_a + m_b)^2}{s} \right)^{1/2} = \frac{2p_{ab}}{\sqrt{s}} \end{aligned} \quad (\text{A.18})$$

and p_{ab} is the magnitude of the 3-momentum of either meson in the center-of-mass system. Note that all expressions are symmetric under the interchange $m_a \rightarrow m_b$. Equation (A.17) with $m_a = m_\pi$ and $m_b = m_\eta$ gives the closed form of $\Pi_{\pi^0\eta}(s)$ for $s > (m_K + m_\eta)^2$.

For equal masses $m_a = m_b = m$, $\Pi(s)$ reduces to the simple form

$$\begin{aligned} \Pi(s) &= \frac{\epsilon}{(4\pi)^2} \left[1 + \ln\left(1 + \frac{\Lambda^2}{m^2}\right) + \frac{m^2}{\Lambda^2} \left(1 + \frac{m^2}{\Lambda^2}\right)^{-1} - 2J(s) \right], \\ J(s) &= \sqrt{-f} \cot^{-1} \sqrt{-f} \theta(4m^2 - s) + \left(\sqrt{f} \tanh^{-1} \sqrt{f} - i\frac{\pi}{2} \sqrt{f} \right) \theta(s - 4m^2) \\ \sqrt{f} &= \left(1 - \frac{4m^2}{s} \right)^{1/2} \end{aligned} \quad (\text{A.19})$$

where the analytic continuation of $J(s)$ into the interval $0 < s < 4m^2$ along the real s axis is also given. Setting $m = m_\pi$ or m_K with $\epsilon = 1/2$ or 1 respectively then leads to closed forms for $\Pi_{\pi\pi}(s)$ and $\Pi_{K\bar{K}}(s)$.

-
- [1] T. Mori *et al.* (Belle Collaboration), Phys Rev. D **75** 051101(R) (2007)
 - [2] S. Uehara *et al.* (Belle Collaboration), Phys Rev. D **78** 052004 (2008)
 - [3] S. Uehara *et al.* (Belle Collaboration), Phys Rev. D **80** 032001 (2009)
 - [4] S. Uehara *et al.* (Belle Collaboration) Prog. Theor. Exp. Phys. 2013, 123C01 (2013).
 - [5] H. Marsiske *et al.* (Crystal Ball Collaboration), Phys. Rev. D **41**, 3324 (1990).
 - [6] T. Oest *et al.* (JADE Collaboration), Z. Phys. C **47**, 343 (1990).
 - [7] B. Hyams *et al.*, Nucl. Phys. B **64**, 134 (1973); G. Grayer *et al.*, Nucl. Phys. B **75**, 189 (1974); B. Hyams *et al.*, Nucl. Phys. B **100**, 205 (1975).
 - [8] D. Cohen, D. S. Ayres, R. Diebold, S. L. Kramer, A. J. Pawlicki, and A. B. Wicklund, Phys. Rev. D **22**, 2595 (1980).
 - [9] A. Etkin *et al.*, Phys. Rev. D **25**, 1786 (1982).
 - [10] J. R. Batley *et al.* (NA48/2 Collaboration), Eur. Phys. J. C **52**, 875 (2007); **54**, 411 (2008); **70**, 635 (2010).
 - [11] R. García-Martín, R. Kamiński, J. R. Peláez, J. Ruiz de Elvira, and F. J. Ynduráin, Phys. Rev. D **83**, 074004 (2011); R. Kamiński, J. R. Peláez, and F. J. Ynduráin, Phys. Rev. D **77**, 054015 (2008); *ibid.* Phys. Rev. D **74**, 014001 (2006); **74**, 079903(E) (2006); J. R. Peláez and F. J. Ynduráin, Phys. Rev. D **71**, 074016 (2005).
 - [12] N. N. Achasov and G. N. Shestakov, JETP Letters **96**, 493 (2012); *ibid.* Physics–Uspekhi **54**, 799 (2011).
 - [13] M. R. Pennington, T. Mori, S. Uehara and Y. Watanabe, Eur. Phys. J. C **56**, 1 (2008).
 - [14] Ling-Yun Dai and M. R. Pennington, Phys. Rev. D **90**, 036004 (2014).
 - [15] L. Montanet, Nucl. Phys. B (Proc. Suppl.) **86**, (2000) 381; V.V. Anisovich, L. Montanet and V.N. Nikolov, Phys. Lett. B **480**, 19 (2000).
 - [16] N. A. Tornquist and M. Roos, Phys. Rev. Lett. **76**, 1575 (1996).
 - [17] V. Dmitrasinović, Phys. Rev. C **53**, 1383 (1996).
 - [18] R. Delbourgo and M. D. Scadron, Int. J. Mod. Phys. A **13**, 657 (1998).
 - [19] M. D. Scadron, G. Rupp, F. Kleefeld, and E. van Beveren, Phys. Rev. D **69**, 014010 (2004); Erratum, Phys. Rev. D **69**, 059901 (2004).
 - [20] N. N. Achasov and V. N. Ivanchenko, Nucl. Phys. B **315**, 465 (1989).
 - [21] J. Weinstein and N. Isgur, Phys. Rev. Lett. **48**, 659 (1982); *ibid.* Phys. Rev. D **27**, 588 (1983); *ibid.* Phys. Rev. D **41**, 2236 (1990).
 - [22] T. Barnes, Phys. Lett. B **165**, 434 (1985).
 - [23] D. Lohse, J. W. Durso, K. Holinde and J. Speth, Nucl. Phys. A **516**, 513 (1990); G. Janssen, B. C. Pearce, K. Holinde and J. Speth, Phys. Rev. D **52**, 2690 (1995).
 - [24] J. A. Oller, Nucl. Phys. A **714**, 161 (2003).
 - [25] S. Krewald, R. H. Lemmer and F. P. Sassen, Phys. Rev. D **69**, 016003 (2004).
 - [26] T. Branz, T. Gutsche and V.E. Lyubovitskij, Eur. Phys. J. A **37**, 303 (2008).
 - [27] R. H. Lemmer, Phys. Rev. C **80**, 045205 (2009).
 - [28] S. Wycech and A. M. Green, Nucl. Phys. A **562**, 446 (1993).
 - [29] B. Kerbikov, Z. Phys. A, **353**, 113 (1995).
 - [30] S. V. Bashinsky and B. Kerbikov, Phys. Atom. Nucl. **59**, 1979 (1996).
 - [31] S. P. Klevansky and R. H. Lemmer, Phys. Lett. B **702**, 235 (2011).
 - [32] J. Gasser and H. Leutwyler, Ann. Phys. **158**, 142 (1984); *ibid.* Nucl. Phys. B **250** 465 (1985).
 - [33] G. Ecker, Prog. Part. Nucl. Phys. **35**, 1 (1995).
 - [34] J. A. Oller and E. Oset, Nucl. Phys. A **620**, (1997) 438; Erratum, *ibid.* Nucl. Phys. A **652**, (1999) 407.
 - [35] J.A. Oller and E. Oset, Nucl. Phys. A **629**, 739 (1998)
 - [36] H. Albrecht *et al.* (ARGUS Collaboration), Z. Phys. C **48**, 183 (1990).
 - [37] J. F. Donoghue and B. R. Holstein, Phys. Rev. D **48**, 137 (1993).
 - [38] See, for example, F. Halzen and A. D. Martin, *Quarks and Leptons* (John Wiley and Sons, New York, 1984).
 - [39] J. L. Peterson, Phys. Rep. **C 2**, 158 (1971).
 - [40] K. Nakamura *et al.* (Particle Data Group) J. Phys G: Nucl. Part. Phys. **37**, 075021 (2010); J. Beringer *et al.* (Particle Data Group), Phys. Rev. D **86**, 010001 (2012) and 2013 partial updates for the 2014

edition.

- [41] Ch. Berger and W. Wagner, *Physics Reports* **146**, 1 (1987).
- [42] M. Abramowitz and I. A. Stegun, Editors, *Handbook of Mathematical Functions* (Dover Publications, Inc., New York, 1965).
- [43] A. R. Edmonds, *Angular Momentum in quantum Mechanics* (Princeton University Press, Princeton, 1960).
- [44] Since we define the vertex diagrams by iV_{ij} the sign of this V_{ij} is the negative of those listed in [34].
- [45] Some authors e.g. [23, 34], include an additional normalization of $1/\sqrt{2}$ in the definition of $|\pi\pi\rangle^0$. Hence the matrix elements V_{ij}^0 given in Eq. (A.16) are larger by a factor $\sqrt{2}$ than those listed by Oller and Oset for each pion label 2 appearing on the interaction matrix element for $I = 0$.